Electronic Supplementary Information (ESI) for

Remarkably Enhanced Proton Conduction of $\{NBu_2(CH_2COOH)_2\}[MnCr(ox)_3]$ by Multiplication of Carboxyl Carrier in the Cation

Hisashi Ōkawa,*[a,b] Kazuya Otsubo,*[a] Yukihiro Yoshida[a] and Hiroshi Kitagawa*[a]

[a]Division of Chemistry, Graduate School of Science, Kyoto University, Kitashirakawa-Oiwakecho, Sakyo-ku, Kyoto 606-8502, Japan

Email: okawa134@outlook.jp, kazuya@kuchem.kyoto-u.ac.jp,

kitagawa@kuchem.kyoto-u.ac.jp

[b]Department of Chemistry, Graduate School of Science, Kyushu University, 744 Motooka, Nishi-ku, Fukuoka 819-0395, Japan

Preparation of {$NBu_2(CH_2COOH)_2$}[$MnCr(ox)_3$] (*dic*-*MnCr*)

A mixture of $(NH_4)_3[Cr(ox)_3]\cdot 3H_2O$ (215 mg), $MnCl_2\cdot 4H_2O$ (100 mg) and $\{NBu_2(CH_2COOH)_2\}Br$ (170 mg) in methanol (15 cm^3) was stirred at ambient temperature to form bluish purple microcrystals. The obtained microcrystals were separated and washed with a small amount of methanol. The yield was 165 mg after dried in air. Anal. Calcd for $\{NBu_2(CH_2COOH)_2\}[MnCr(ox)_3]$ ($C_{18}H_{24}CrMnNO_{16}$) (%): C, 35.02: H, 3.92; N, 2.27. Found (%): C, 35.30; H, 4.16; N, 2.34. Mn/Cr = 1.04 from X-ray fluorescence spectroscopy (Rigaku, ZSX Primus IV).

Physical Measurements

X-ray powder diffraction (XRPD) pattern was measured using Bruker D8 ADVANCE diffractometer. Fourier transform infrared (FTIR) spectra were collected from KBr pellets using Thermo Fisher NEXUS 670 FTIR spectrometer. Thermogravimetric analysis (TGA) was performed using Bruker TG-DTA 2000SA with heating rate of 5 °C/min under N_2 gas flow (100 mL/min). Proton conductivity measurements on compacted pellets (~10 mg, ~0.8 mm thickness × 2.5 mm ϕ) were carried out using a Solartron 1260 Impedance/Gain–Phase Analyzer and 1296 Dielectric Interface in the frequency range 1 Hz–1 MHz. Relative humidity was controlled using an Espec Corp. SH-221. Water adsorption isotherm was collected at 298 K with BELSORP-max (BEL JAPAN). Samples (~100 mg) were thoroughly dehydrated prior to the measurement by heating at 373 K for 24 h under vacuum.

X-ray powder diffraction analysis for *dic-MnCr*

Fig. S1 shows XRPD patterns of ***dic***-*MnCr* and ***moc***-*MnCr*. As clearly observed, ***dic***-*MnCr* shows poor crystallinity, but its diffraction pattern is very similar to that of previously reported ***moc***-*MnCr*[S1] indicating that ***dic***-*MnCr* is composed of two-

dimensional (2D) MnCr bimetallic (anionic) frameworks and organic cations (*AcBu*$_2$-*stratum*). Le Bail fitting on the experimental XRPD pattern (Fig. S2) led to similar lattice constants (Trigonal, *R*3*c*, *a* = 9.273(5)Å, *c* = 50.98(3) Å and *V* = 3796(4) Å^3) to those of ***moc***-*MnCr*. To obtain further information on the crystal structure of ***dic***-*MnCr*, ab initio structure solution was carried out by simulated annealing method installed on EXPO2014[S2] program. In this analysis, 2D MnCr bimetallic (anionic) framework with one *AcBu*$_2$-*stratum* unit was used as initial structure model. A total of 30 cycles calculation which consists of each ~5 × 10^6 Monte Carlo moves of *AcBu*$_2$-*stratum* unit gave good structural model shown in Fig. 1. In this structural solution in simulated annealing method, carboxylate- and butyl-groups are disordered (see Fig. 1 in the main text). Rietveld refinement using this structural model was not successful because of poor crystallinity.

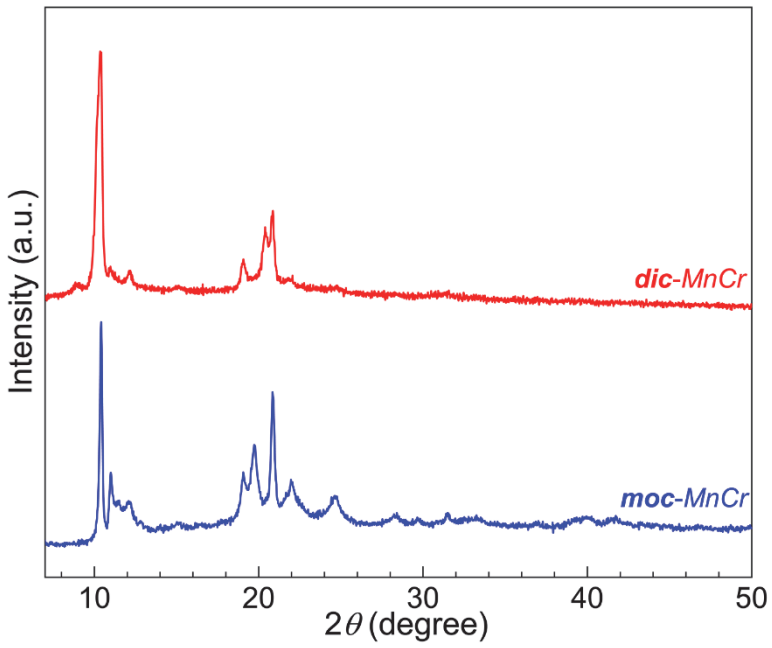

Fig. S1 XRPD patterns (Cu *K*α radiation) of ***dic***-*MnCr* (red) and ***moc***-*MnCr* (blue) at room temperature (RT).

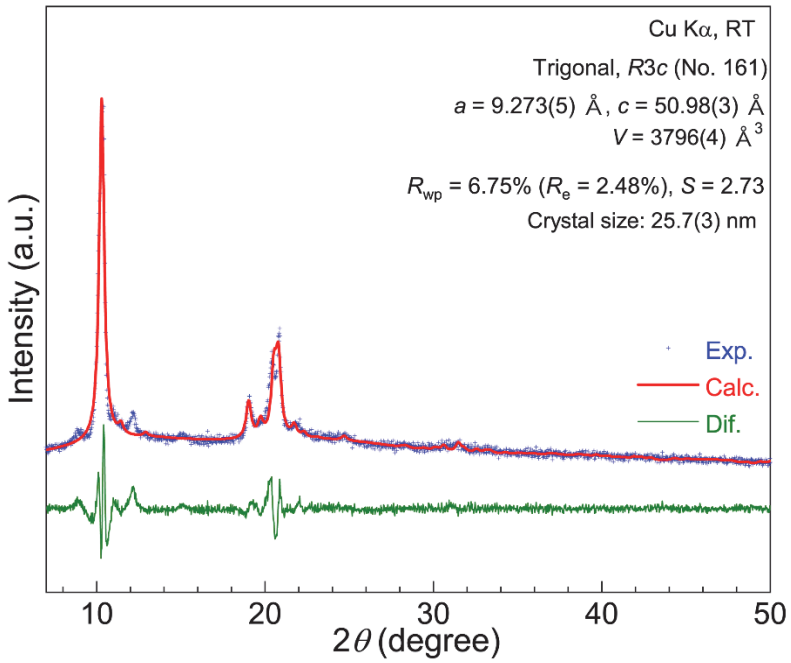

Fig. S2 Le Bail fitting result on ***dic*-*MnCr***. Blue crosses, red line, and thin green line denote experimental, calculated, and difference profiles, respectively.

FTIR spectra

Fig. S3 shows FTIR spectrum of ***dic*-*MnCr***. For comparison, FTIR spectra of $(NBu_4)[MnCr(ox)_3]$[S3] and $(NH_4)_2(adp)[Zn(ox)_3]$[S4] having $M_2(ox)_3$ (M: metal ion) 2D honeycomb layer structure are also shown. For ***dic*-*MnCr***, typical ν(C=O) mode of the ox ligand in 2D ox-bridged networks was observed at 1632 cm^{-1}. Weak peak at 1743 cm^{-1} can be assigned to the ν(C=O) mode of the *AcBu₂-stratum* unit. In addition, the $\delta(CH_2)$ and $\gamma(CH_2)$ modes of the *n*-butyl group of the *AcBu₂-stratum* unit were observed around 1400 cm^{-1}. The ν(C-H) stretching mode of the *n*-butyl group could be observed as broad and weak band around 3000 cm^{-1}. The similarity of the spectral feature to those of reference compounds clearly indicates that ***dic*-*MnCr*** is composed of 2D MnCr bimetallic (anionic) framework.

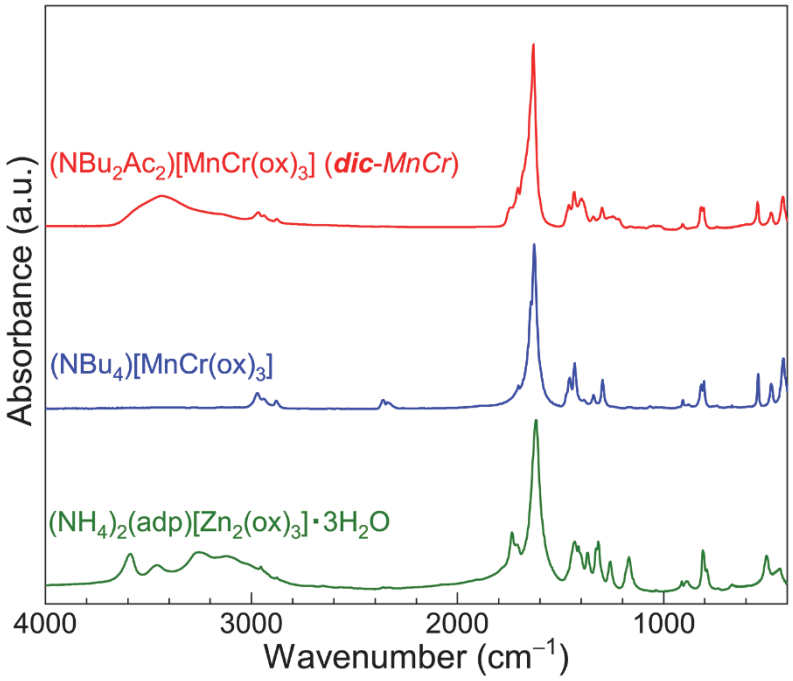

Fig. S3 FTIR spectra of ***dic***-*MnCr*, $(NBu_4)[MnCr(ox)_3]$[S3] and $(NH_4)_2(adp)[Zn(ox)_3]$[S4] at RT.

TGA analysis

TGA curve of ***dic***-*MnCr* (powder sample, 5.44 mg) is shown in Fig. S4. Previously, the thermal decomposition of analogue compound, $(NBu_4)[MnCr(ox)_3]$ was examined in detail.[S5] According to this report, thermal conversion of $(NBu_4)[MnCr(ox)_3]$ occurs at about 400 °C in one step providing the bimetallic oxide, $Mn_{1.5}Cr_{1.5}O_4$. As clearly seen in Fig. S4, similar one-step thermal decomposition was observed above 300 °C. At 400 °C, observed weight loss reached about 67% (~3.64 mg), which is consistent with the calculated weight loss (64%, ~3.48 mg) in the formation of $Mn_{1.5}Cr_{1.5}O_4$. This result supports the purity of the ***dic***-*MnCr* sample obtained.

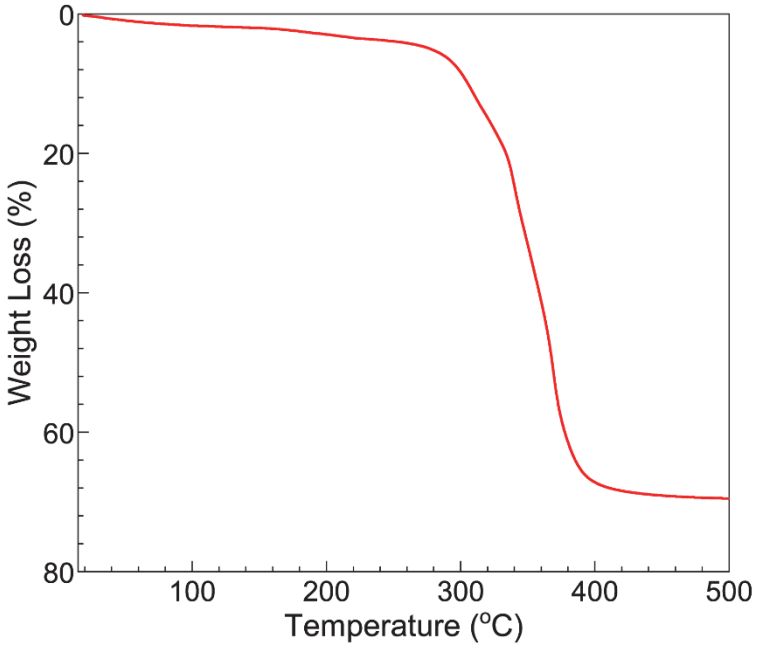

Fig. S4 Thermogravimetric analysis of ***dic***-*MnCr*.

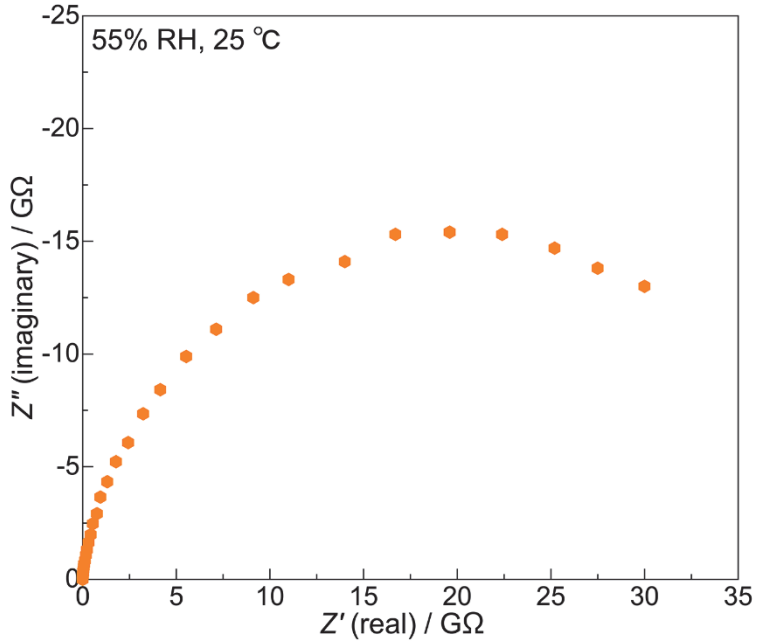

Fig. S5 Selected Nyquist plots in the complex plane of ***dic***-*MnCr* at 55% RH at 25 °C.

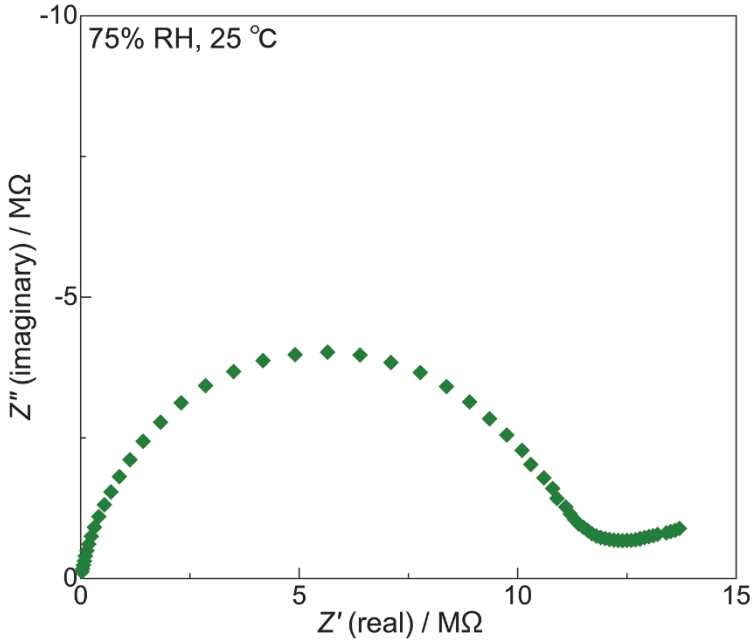

Fig. S6 Selected Nyquist plots in the complex plane of ***dic***-*MnCr* at 75% RH at 25 °C.

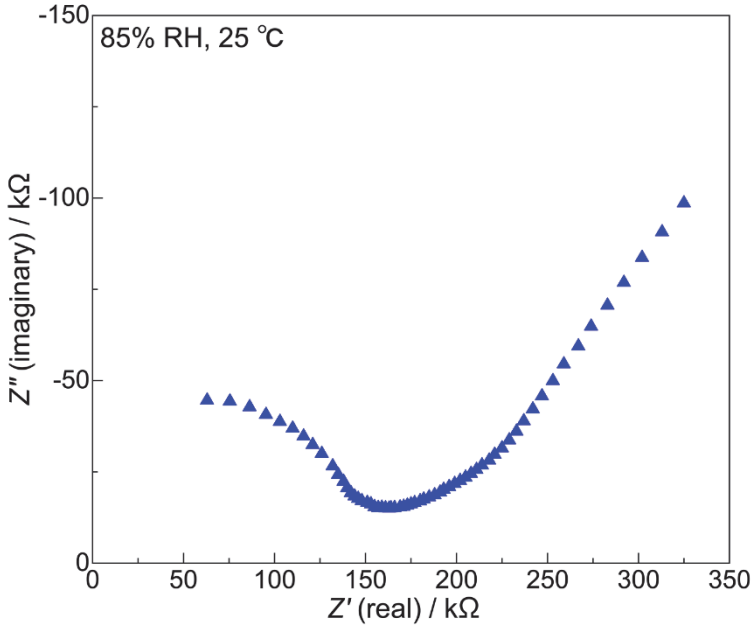

Fig. S7 Selected Nyquist plots in the complex plane of ***dic***-*MnCr* at 85% RH at 25 °C.

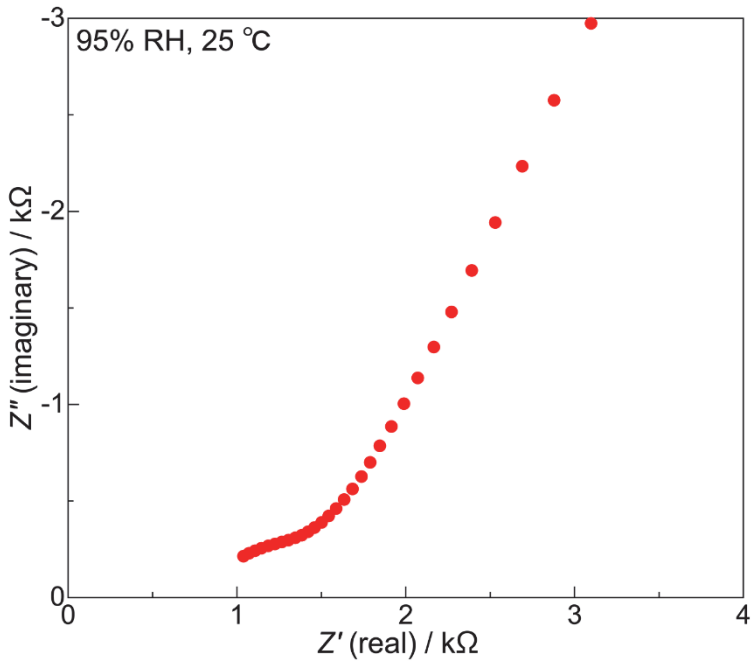

Fig. S8 Selected Nyquist plots in the complex plane of ***dic***-*MnCr* at 95% RH at 25 °C.

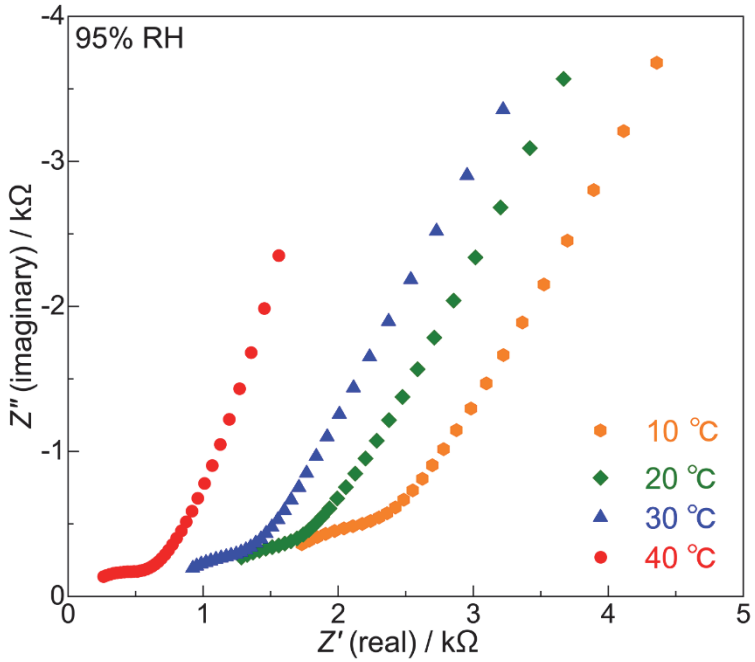

Fig. S9 Temperature dependence of Nyquist plots of ***dic***-*MnCr* at 95% RH.

Structure under humidified condition

To obtain the structural information of fully hydrated form of ***dic***-*MnCr*, XRPD pattern was collected on the sample humidified at 97% RH (Fig. S10). As clearly observed, hydrated ***dic***-*MnCr* showed similar XRPD pattern to that of non-hydrated form, but the several diffraction peaks were shifted to lower angle side. Especially, the 006 diffraction peak (corresponding to the MnCr 2D layer stacking direction) was largely shifted, which suggests intercalation of water molecules between the layers. From the shift of 006 peak, the expansion of interlayer spacing can be estimated to be ~1.4%. Besides, several additional diffraction peaks were observed in hydrated form. Due to poor crystallinity of the sample, few diffraction peaks could be detected. Although further structural analyses on hydrated form were not successful at present stage, these results implied water vapour induced structural transition (such as disorder ↔ order transition).

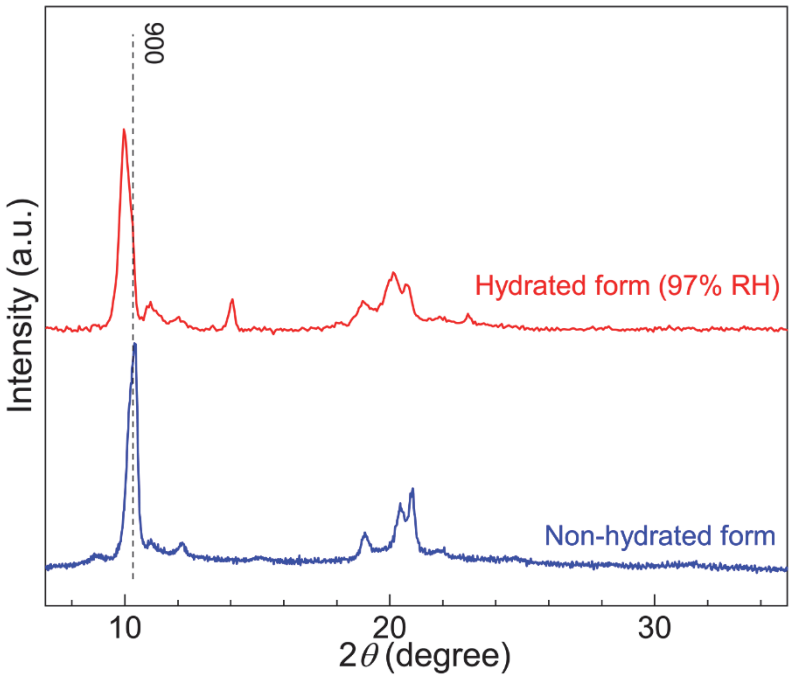

Fig. S10 XRPD patterns (Cu *K*α radiation) of ***dic***-*MnCr* in different states at RT.

References for ESI

(S1) (a) M. Sadakiyo, H. Ōkawa, A. Shigematsu, M. Ohba, T. Yamada and H. Kitagawa, *J. Am. Chem. Soc.*, 2012, **134**, 5472; (b) H. Ōkawa, M. Sadakiyo, T. Yamada, M. Maesato, M. Ohba and H. Kitagawa, *J. Am. Chem. Soc.*, 2013, **135**, 2256.

(S2) A. Altomare, C. Cuocci, C. Giacovazzo, A. Moliterni, R. Rizzi, N. Corriero and A. Falcicchio, *J. Appl. Cryst.* 2013, **46**, 1231.

(S3) H. Tamaki, Z. J. Zhong, N. Matsumoto, S. Kida, M. Koikawa, N. Achiwa, Y. Hashimoto and H. Ōkawa, *J. Am. Chem. Soc.*, 1992, **114**, 6974.

(S4) M. Sadakiyo, T. Yamada and H. Kitagawa, *J. Am. Chem. Soc.*, 2009, **131**, 9906.

(S5) K. E. Neo, Y. Y. Ong, H. V. Huynh and T. S. A. Hor, *J. Mater. Chem.*, 2007, **17**, 1002.